V. 119, NO. 5
SEPTEMBER 2022

ACI STRUCTURAL JOURNAL

A JOURNAL OF THE AMERICAN CONCRETE INSTITUTE

American Concrete Institute

CONTENTS

PRINTED WITH SOY INK

ACI Structural Journal

September 2022, V. 119, No. 5

A JOURNAL OF THE AMERICAN CONCRETE INSTITUTE
AN INTERNATIONAL TECHNICAL SOCIETY

Contents continued on next page

Discussion is welcomed for all materials published in this issue and will appear ten months from this journal's date if the discussion is received within four months of the paper's print publication. Discussion of material received after specified dates will be considered individually for publication or private response. ACI Standards published in ACI Journals for public comment have discussion due dates printed with the Standard.

The *ACI Structural Journal* (ISSN 0889-3241) is published bimonthly by the American Concrete Institute. Publication office: 38800 Country Club Drive, Farmington Hills, MI 48331. Periodicals postage paid at Farmington, MI, and at additional mailing offices. Subscription rates: $189 per year, payable in advance. POSTMASTER: Send address changes to: *ACI Structural Journal*, 38800 Country Club Drive, Farmington Hills, MI 48331.

Canadian GST: R 1226213149.

Direct correspondence to 38800 Country Club Drive, Farmington Hills, MI 48331. Telephone: +1.248.848.3700. Facsimile (FAX): +1.248.848.3701. **Website: http://www.concrete.org.**

CONTENTS

ON COVER: 119-S104, p. 101, Fig. 8—Test setup for both test specimens.

Contributions to *ACI Structural Journal*

The *ACI Structural Journal* is an open forum on concrete technology and papers related to this field are always welcome. All material submitted for possible publication must meet the requirements of the "American Concrete Institute Publication Policy" and "Author Guidelines and Submission Procedures." Prospective authors should request a copy of the Policy and Guidelines from ACI or visit ACI's website at **www.concrete.org** prior to submitting contributions.

Papers reporting research must include a statement indicating the significance of the research.

The Institute reserves the right to return, without review, contributions not meeting the requirements of the Publication Policy.

All materials conforming to the Policy requirements will be reviewed for editorial quality and technical content, and every effort will be made to put all acceptable papers into the information channel. However, potentially good papers may be returned to authors when it is not possible to publish them in a reasonable time.

Discussion

All technical material appearing in the *ACI Structural Journal* may be discussed. If the deadline indicated on the contents page is observed, discussion can appear in the designated issue. Discussion should be complete and ready for publication, including finished, reproducible illustrations. Discussion must be confined to the scope of the paper and meet the ACI Publication Policy.

Follow the style of the current issue. Be brief—1800 words of double spaced, typewritten copy, including illustrations and tables, is maximum. Count illustrations and tables as 300 words each and submit them on individual sheets. As an approximation, 1 page of text is about 300 words. Submit one original typescript on 8-1/2 x 11 plain white paper, use 1 in. margins, and include two good quality copies of the entire discussion. References should be complete. Do not repeat references cited in original paper; cite them by original number. Closures responding to a single discussion should not exceed 1800-word equivalents in length, and to multiple discussions, approximately one half of the combined lengths of all discussions. Closures are published together with the discussions.

Discuss the paper, not some new or outside work on the same subject. Use references wherever possible instead of repeating available information.

Discussion offered for publication should offer some benefit to the general reader. Discussion which does not meet this requirement will be returned or referred to the author for private reply.

Send manuscripts to:
http://mc.manuscriptcentral.com/aci

Send discussions to:
Journals.Manuscripts@concrete.org

ACI STRUCTURAL JOURNAL TECHNICAL PAPER

Title No. 119-S104

Moment Transfer at Column-Foundation Connections: Physical Tests

by Benjamin L. Worsfold, Jack P. Moehle, and John F. Silva

Steel and precast columns are commonly designed to transfer moment loads to concrete foundations through cast-in-place headed anchors. In design office practice in the United States, connection strength has been evaluated considering mechanisms emphasizing joint shear, strut-and-tie modeling, and anchoring to concrete. For any given connection, the strengths calculated with these three methods can differ by a wide margin. The application of these methods, including possible enhancements that improve strength estimates, is described. Laboratory tests were performed to provide benchmark physical data to determine the applicability of various design methods. The test specimens consisted of full-scale interior steel-column-to-concrete-foundation connections located away from foundation edges, with details typical of current construction practice on the West Coast of the United States. Strength in both tests was governed by concrete breakout failure. Strategically placed reinforcement increased the strength and displacement capacity of anchored connections governed by breakout. Design recommendations are provided.

Keywords: anchoring to concrete; beam-column joint; breakout; column-foundation connections; shear reinforcement; strut-and-tie; supplementary reinforcement.

INTRODUCTION

Connections between structural columns and foundations are common in building construction. Whether the column is cast-in-place concrete, precast concrete, or structural steel, moment transfer at the foundation presents a challenge for designers as little consensus exists regarding what failure modes are relevant or which design provisions apply. This paper describes three moment transfer models that have been considered by practicing structural engineers for steel columns anchored to foundations using cast-in-place anchors. These are: 1) anchoring-to-concrete provisions (for example, ACI 318-19, Chapter 17 [ACI Committee 318 2019]); 2) strut-and-tie modeling (for example, ACI 318-19, Chapter 23); and 3) joint-shear design provisions (for example, ACI 352R-02 [ACI Committee 352 2002]). For any given connection, the strengths calculated with these three methods can differ by a large margin.

The ACI anchoring-to-concrete provisions historically reflect larger safety margins than is common in other parts of the Code. This is in part due to the potential for a "single-point fastening," whereby loads can be carried by a connection providing no redundancy and little warning of failure. Various options for reducing conservatism are discussed, such as including the beneficial effect of column flexural compression and the use of a median breakout strength rather than a 5% fractile value. These measures may allow designers to consider breakout failure in a manner that is more consistent with other methods and may lead to more economical designs while preserving the overall required reliability.

Two full-scale interior steel-column-to-concrete-foundation connections located away from foundation edges were constructed and tested under reversed-cyclic lateral loading to better understand the failure mechanisms and design requirements. One of the test specimens was constructed without transverse reinforcement in the foundation, while the other test specimen had transverse reinforcement to increase strength and deformation capacity. Design recommendations are made based on the test results.

LITERATURE REVIEW

Fuchs et al. (1995) proposed the Concrete Capacity Design (CCD) method as a simplified model for calculating the peak breakout strength of anchors or anchor groups in plain concrete. This method forms the basis for many modern building codes, including ACI 318 and EN 1992-4 (2018). Tests have shown that the breakout force does not increase linearly with the size of the failure area (Ožbolt et al. 1999). This phenomenon is attributed to the size effect in concrete fracture (Eligehausen et al. 1992; Bažant 2000) and is incorporated into the CCD method by modifying the exponent on the effective depth. If the size effect is not considered, the breakout strength predicted for anchors with larger embedment may be unconservative.

Tests on anchors in cracked concrete tend to result in lower breakout strengths and lower stiffnesses than anchors tested in so-called uncracked concrete (Eligehausen et al. 2006). Eligehausen and Balogh (1995) report that preexisting cracks extending through the full anchor depth with a uniform crack width between 0.3 to 0.4 mm can reduce tension capacity governed by concrete breakout by approximately 25% (headed and undercut anchors) or 35% (torque-controlled expansion anchors) compared to the uncracked conditions. These researchers recommend that, in general, the design of anchors should assume the cracked condition.

ACI 352R-02 describes recommendations for designing monolithic beam-column connections for structural frames. The geometry and force flow of a column-foundation

ACI Structural Journal, V. 119, No. 5, September 2022.

MS No. S-2021-128.R3, doi: 10.14359/51734799, received February 11, 2022, and reviewed under Institute publication policies.

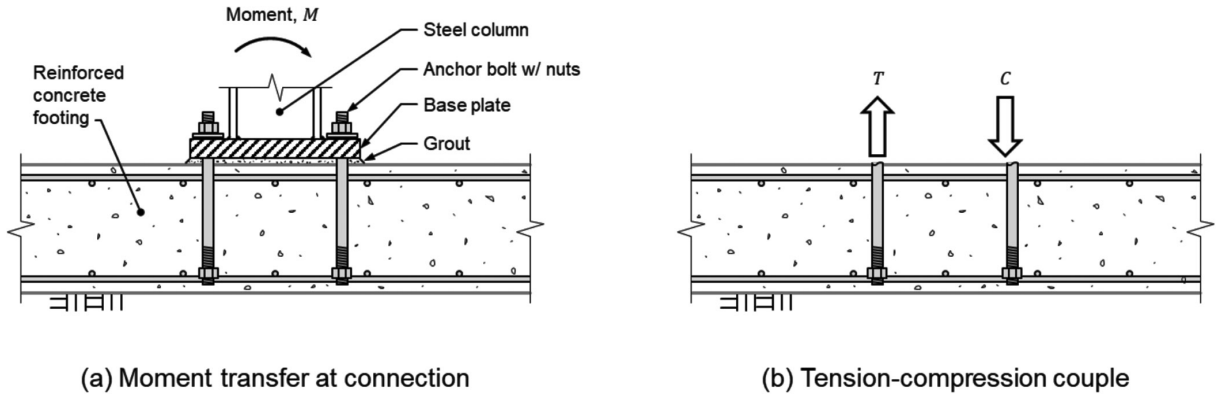

Fig. 1—Moment transfer between steel wide-flange column and reinforced concrete foundation.

connection can be thought of as similar to a roof connection confined on all four sides. Therefore, some engineers use the ACI 352R-02 recommendations for the design of column-foundation connections.

Tanaka and Oba (2001) tested six concrete column-foundation connections comparing columns anchored with cast-in bent-out hooks and post-installed bonded reinforcing bars. Specimens governed by concrete cone failure show low displacement capacity and pinched hysteresis loops. The researchers also noted that the embedment of post-installed reinforcing bars required to avoid breakout failure was less than the prescribed development lengths.

Based on 16 full-scale column-foundation connection specimens and analytical simulations, Mahrenholtz et al. (2014) propose a design method that enhances the ACI 318-19 (ACI Committee 318 2019) breakout strength equations. Two modification factors are proposed to consider: 1) the degradation due to cyclic loading; and 2) the beneficial effect of the column flexural compressive force, which constrains the formation of the traditional breakout cone (as proposed by Herzog [2015]).

Multiple researchers have investigated the beneficial effect of different reinforcement configurations on anchor behavior. Sharma et al. (2017a,b) described a series of physical tests of anchor groups with so-called supplementary reinforcement under tensile loads or shear loads toward an edge. They showed that relatively small amounts of reinforcement increase anchor group strength and displacement capacity. Based on finite element simulations (Nilforoush et al. 2017) and physical experiments (Nilforoush et al. 2018), a modification factor was proposed to consider the beneficial effect of surface reinforcement on breakout failure. However, no additional benefit was observed for surface reinforcement ratios above 0.3%. Papadopoulos et al. (2018) investigated headed reinforcing bars in column-slab connections for bridges. They demonstrated that shear reinforcement in the form of J-bars inside the joint and stirrups outside the joint prevented breakout failure and punching of the heads through the far side of the slab. The first row of stirrups outside the joint improved the behavior of the connection, while additional rows seemed to have no effect. The results led to detailing recommendations adopted by the California Department of Transportation (Caltrans) in MTD 20-7 (Caltrans 2016).

RESEARCH SIGNIFICANCE

Full-scale laboratory tests of column-foundation connections with cast-in-place headed anchors focusing on the concrete failure modes are scarce, particularly for deep anchors where $h_{ef} > 10$ in. (250 mm). This project also investigates the influence of distributed reinforcing bars across the breakout failure zone. This research project provides benchmark physical data and evaluates alternate design methods.

FORCE TRANSFER AT COLUMN-FOUNDATION CONNECTIONS

Figure 1 illustrates an idealized case of a steel column transferring pure moment (no shear or axial loads) into a reinforced concrete foundation through a base plate and anchor bolts. In Fig. 1(a), it is assumed that there are two lines of bolts, one on each side of the column. The moment is resisted by a tension-compression couple, as shown in Fig. 1(b). The tensile force T is resisted directly by the line of anchor bolts on the left side of the connection. The compressive force C is resisted by compression between the base plate and the grout-concrete interface. In a typical foundation, these actions are transferred into the foundation, which, in turn, transfers them to the surrounding soil and foundation elements.

A fundamental design question is: "How is the tension-compression couple formed by T and C resolved in the concrete in the immediate vicinity of the applied forces, and how should the connection be assessed for structural adequacy?" The following three design options are considered herein:

1. Design the connection using current design rules for beam-column joints.
2. Design the connection using a strut-and-tie model.
3. Design the connection considering anchoring-to-concrete provisions.

The following text considers each of these connection design options in turn. Moment transfer is assumed to be due to earthquake effects, which will dictate some of the strength and detailing requirements.

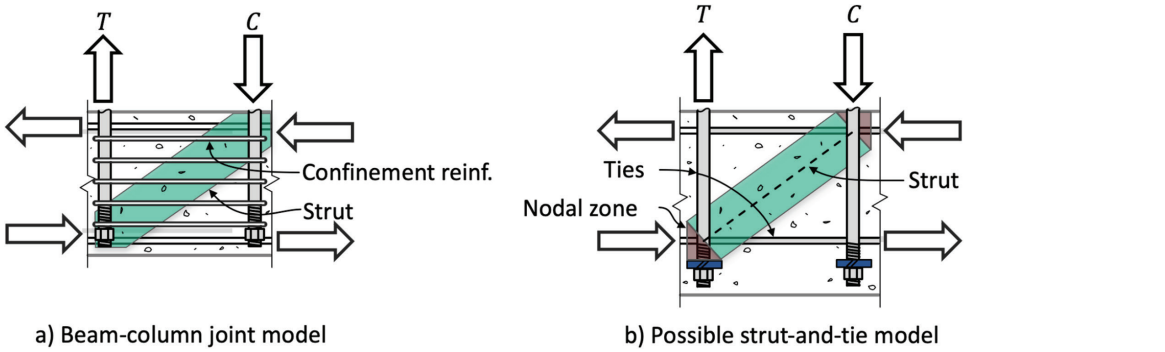

Fig. 2—Column-foundation connection models.

DESIGN AS BEAM-COLUMN JOINT

In this approach, the connection is designed as a beam-column joint following ACI 318-19 or ACI 352R-02 provisions. The joint is defined as the volume of concrete bounded by the depth of the foundation vertically and a horizontal area within the effective bearing area of the base plate. This joint is assumed to transfer horizontal joint shear through a diagonal strut, as shown in Fig. 2(a). Transverse reinforcement is provided following ACI 318-19 or ACI 352R-02 provisions to confine the joint and thereby improve its ability to transmit joint shear under load and deformation reversals. Nominal joint shear strength is defined as

$$V_n = \gamma\sqrt{f_c'}A_j \tag{1}$$

where γ is the joint shear strength coefficient dependent on joint geometry and loading; f_c' is the concrete compressive strength; and A_j is the cross-sectional area of a horizontal plane through the joint. The joint shear strength coefficient is taken as $\gamma = 15$ for psi units (1.2 for SI units) by considering the joint to have all four vertical faces confined and a discontinuous column subjected to lateral loading resulting from ground motion.

DESIGN BY STRUT-AND-TIE METHOD

The strut-and-tie method was developed for regions near geometric discontinuities and points of load application, including beam-column joints. Figure 2(b) illustrates a possible model for the application of the strut-and-tie method, including nodal zones, struts, and ties that are in equilibrium with the forces external to the discontinuity region. To facilitate effective nodal zone development, the anchor bolts may need to extend below the flexural tension-compression zone at the bottom of the foundation and be equipped with plate washers at the ends of the anchor bolts. This extension of the anchor bolts may be impractical from a construction perspective because concrete cover requirements would require thickening the foundation, either globally or locally, with associated cost implications. In a typical application, the discontinuity region might be designed to develop the full tensile strength of the anchor bolts on one side of the joint, with plate washers sized to keep stresses for nodal zones and struts within acceptable limits. According to ACI 318-19, the nominal axial compressive strength of a strut is given by

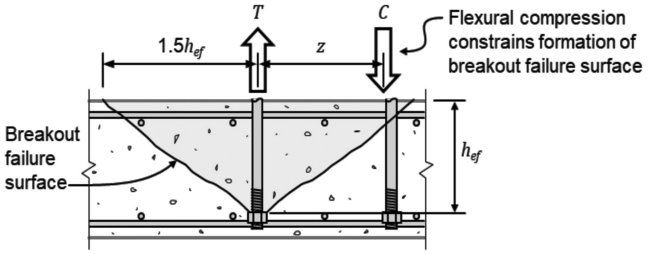

Fig. 3—Breakout failure.

$$F_{ns} = 0.85\beta_c\beta_s f_c' A_{cs} \tag{2}$$

where $\beta_c = 1.0$ because there is no adjacent bearing surface; $\beta_s = 0.75$ for beam-column joints; and A_{cs} is the cross-sectional area at the end of the strut under consideration. The nodal zone at the lower left is anchoring two ties and one strut, making it a compression-tension-tension (C-T-T) node, so its strength is given by

$$F_{nn} = 0.85\beta_c\beta_n f_c' A_{nz} \tag{3}$$

where $\beta_n = 0.60$ for beam-column joints; and A_{nz} is the area of each face of the nodal zone. ACI 318-19, Section 23.11, specifies an additional factor for regions of a seismic force-resisting system assigned to Seismic Design Category D, E, or F. However, if the forces are limited by the yielding of the tension anchor, the additional factor is 1.0.

DESIGN USING ANCHORING-TO-CONCRETE PROVISIONS

The ACI 318-19 provisions for anchoring to concrete include equations to calculate concrete breakout failure, in this case, characterized by cracks initiating at the bearing heads of the tension-loaded anchors and propagating toward the concrete surface at an angle of approximately 34 degrees (1.5:1) from the horizontal, as shown in Fig. 3. This failure mode is recognizable by the appearance of a circular fracture pattern at the concrete surface and the subsequent pyramidal volume of detached concrete. According to ACI 318-19, for a group of anchors, the nominal breakout strength is given by

$$N_{cbg} = \frac{A_{Nc}}{A_{Nco}}\Psi_{ec,N}\Psi_{ed,N}\Psi_{c,N}\Psi_{cp,N}N_b \tag{4}$$

where A_{Nc}/A_{Nco} is the projected concrete failure area for the anchor group divided by the failure area for a single anchor; $\Psi_{ec,N}$ is the breakout eccentricity factor; $\Psi_{ed,N}$ is the breakout edge-effect factor; $\Psi_{c,N}$ is the breakout cracking factor; $\Psi_{cp,N}$ is the splitting modification for post-installed anchors; and N_b is the 5% fractile basic concrete breakout strength of a single anchor

$$N_b = 24\sqrt{f_c'}h_{ef}^{1.5} \text{ (if } h_{ef} \le 11 \text{ in.) (lb, in.)}$$
$$N_b = 10\sqrt{f_c'}h_{ef}^{1.5} \text{ (if } h_{ef} \le 0.28 \text{ m) (SI)} \quad (5)$$

$$N_b = 16\sqrt{f_c'}h_{ef}^{5/3} \text{ (if 11 in.} \le h_{ef} \le 25 \text{ in.) (lb, in.)}$$
$$N_b = 3.9\sqrt{f_c'}h_{ef}^{5/3} \text{ (if 0.28 m} \le h_{ef} \le 0.64 \text{ m) (SI)} \quad (6)$$

where h_{ef} is the depth to the bearing surface of the anchor bolt. For this case, $\Psi_{ec,N} = \Psi_{ed,N} = \Psi_{cp,N} = 1.0$. A value of $\Psi_{c,N} = 1.0$ should be used if the concrete foundation element is expected to exhibit cracking under service loads near the anchors; otherwise, $\Psi_{c,N} = 1.25$. Shallow foundations subjected to large anchor forces associated with seismic demands may develop flexural stresses that exceed the modulus of rupture and, as such, could be considered cracked for anchor design. However, in cases where the anchor bearing surface is located well below the neutral axis, as shown in Fig. 3, the effect of cracking on the anchor breakout strength of a headed bolt is likely to be marginal. For this reason, ACI 318-19, Section 17.10.5.4, specifically permits consideration of the uncracked concrete state, "where it can be demonstrated that the concrete remains uncracked." It seems reasonable to apply this exception here.

Figure 3 illustrates that, for some connection geometries, the flexural compression force resultant C may bear against the failure cone such that the breakout failure will be constrained. This constraint has been observed to increase the breakout strength (Mahrenholtz et al. 2014; Herzog 2015). EN 1992-4:2018 accounts for this effect by incorporating an additional factor in the breakout force calculation

$$\Psi_M = 2 - \frac{z}{1.5h_{ef}} \ge 1.0 \quad (7)$$

where the variable z is the distance between the tensile and compressive resultants (Fig. 3). This effect is not considered in ACI 318-19.

According to ACI 318-19, the nominal strength for an anchor or anchor group is intended to correspond to a 5% fractile of the measured strengths. This design basis is in sharp contrast with the design for other actions covered in the Code, where the nominal strength is intended to correspond more closely with a mean or median strength. To convert a 5% fractile value to a median value, one may assume measured strengths follow a normal distribution with a covariance of 0.15 (Fuchs et al. 1995). The modification factor (f_{mean}) can be calculated using the standard normal distribution z-value for a 5% fractile, $z = -1.645$

Table 1—Concrete properties of foundation slab for both specimens

Specimen	M01	M02
f_c', psi (MPa)	3700 (25.5)	3930 (27.1)
E, ksi (GPa)	3470 (23.9)	3610 (24.9)
f_t, psi (MPa)	380 (2.62)	438 (3.02)
G_f, lb/in. (N/m)	0.310 (54.3)	0.896 (157)
Los Angeles abrasion test, 3/4 in. (19 mm) aggregate	21%	21%

$$f_{mean} = \frac{1}{1 + z \cdot \text{COV}} = \frac{1}{1 + (-1.645) \cdot 0.15} = 1.33 \quad (8)$$

OBSERVATIONS FROM LABORATORY TESTS

Two full-scale column-foundation connection tests were carried out to gain insights into the different design methods described previously and the influence of reinforcing bars on breakout failure. The test specimens comprised a steel wide-flange column connected to a foundation slab by cast-in-place anchor bolts (refer to Fig. 4 to 7). The column was subjected to reversed-cyclic lateral loads with no additional axial load other than self-weight. Worsfold and Moehle (2019, 2022) provide detailed descriptions of the test specimens and experimental results for Specimens M01 and M02, respectively.

Test specimen design—Specimen M01

Test Specimen M01 was designed so that strength would be limited by the failure of the concrete foundation in the connection region. The steel column (W12x106 ASTM A992 Grade 50) was welded to a 2-3/4 in. (70 mm) thick base plate (ASTM A529 Grade 50) with a 5.25 x 5.25 x 2 in. (133 x 133 x 50 mm) shear lug (ASTM A529 Grade 50) and a 0.75 in. (19 mm) layer of non-shrink grout. Four 1-1/2 in. (38 mm) diameter anchor bolts (ASTM F1554 Grade 105) with heavy hex nuts as heads were cast into the 18 in. (457 mm) thick foundation on each side of the column with an effective embedment depth from the top of the slab to the bearing surface equal to 14.3 in. (363 mm). Note that this embedment depth does not place the bearing surface of the nuts below the slab flexural reinforcement as may be required by some strut-and-tie models (refer to Fig. 2(b)). The bearing area of each heavy hex nut was 2.6 in.^{2} (1690 mm^2).

The foundation slab was designed to resist the shear and moment resulting from developing the column moment yield strength. The normalweight concrete had a nominal maximum aggregate size of 3/4 in. (19 mm) and a measured a compressive strength of 3700 psi (25.5 MPa) on test day. The compressive strength (f_c'), modulus of elasticity (E), and tensile capacity (f_t) were measured from 6 x 12 in. (152 x 305 mm) concrete cylinders (refer to Table 1). The fracture energy (G_f) was measured with three-point bending tests following RILEM recommendations TC 89-FMC 2 (RILEM TC 89 1994). Refer to Worsfold and Moehle (2019) for further details on measured material properties, including stress-strain curves for concrete and reinforcing bars. Slab flexural reinforcement was sized assuming nominal yield

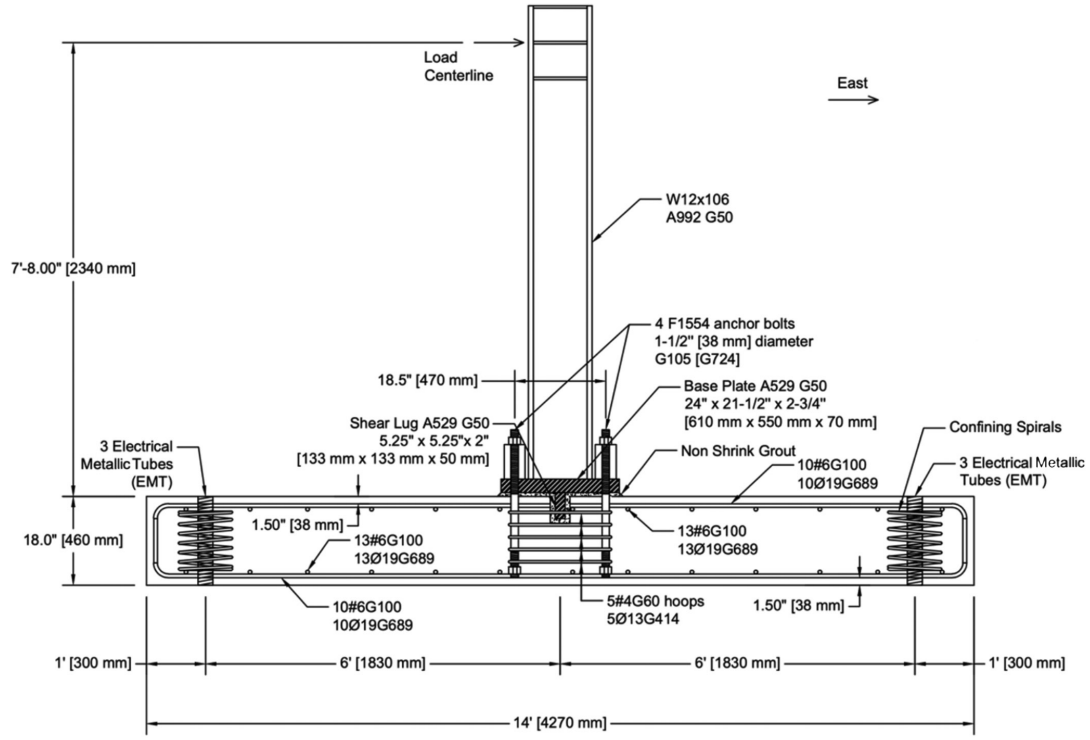

Fig. 4—Specimen M01 elevation view.

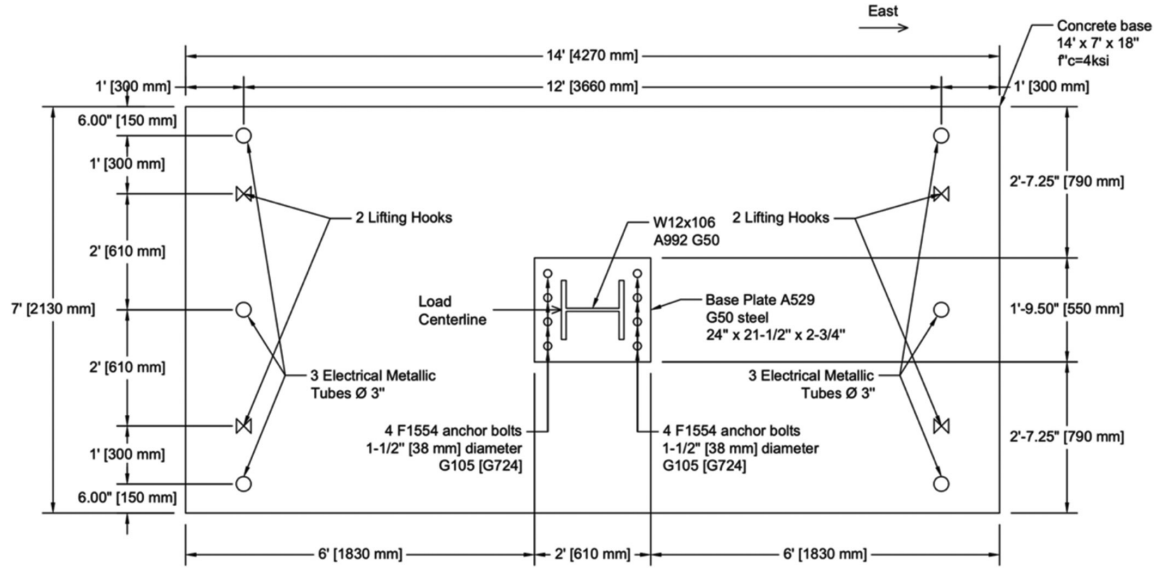

Fig. 5—Specimen M01 plan view.

strength f_y = 60,000 psi (420 MPa). However, Grade 100 (690 MPa) reinforcement was substituted to guard against yielding in case unexpected overloads or localized stress concentrations occurred. The joint was confined with five No. 4 (Ø13 mm) Grade 60 (420 MPa) hoops, consistent with the requirement of ACI 352R-02 for beam-column joint confinement, as well as requirements for distributed strut reinforcement from the ACI 318-19 strut-and-tie method.

The steel column was subjected to quasi-static reversed-cyclic lateral load applied at an elevation H = 7 ft 8 in. (2.34 m) above the top of the foundation slab in the strong direction of the column (east-west). Each load step involved two load cycles to a given drift ratio in the positive and negative directions. The test was paused when each new displacement goal was reached to document cracking. Axial load was limited to self-weight as this is a critical case for breakout failure, which simplifies the testing apparatus.

The slab was simply supported at the ends where it was post-tensioned to bearing pads located 6 ft (1.83 m) from the center of the column to provide sliding and overturning resistance. Note that these support conditions are different from those in a soil-supported foundation. The selected boundary conditions simplify the test and the interpretation of the test results and are unlikely to affect the breakout failure mode observed for the test specimen. Figure 8 shows a photograph of the test setup.

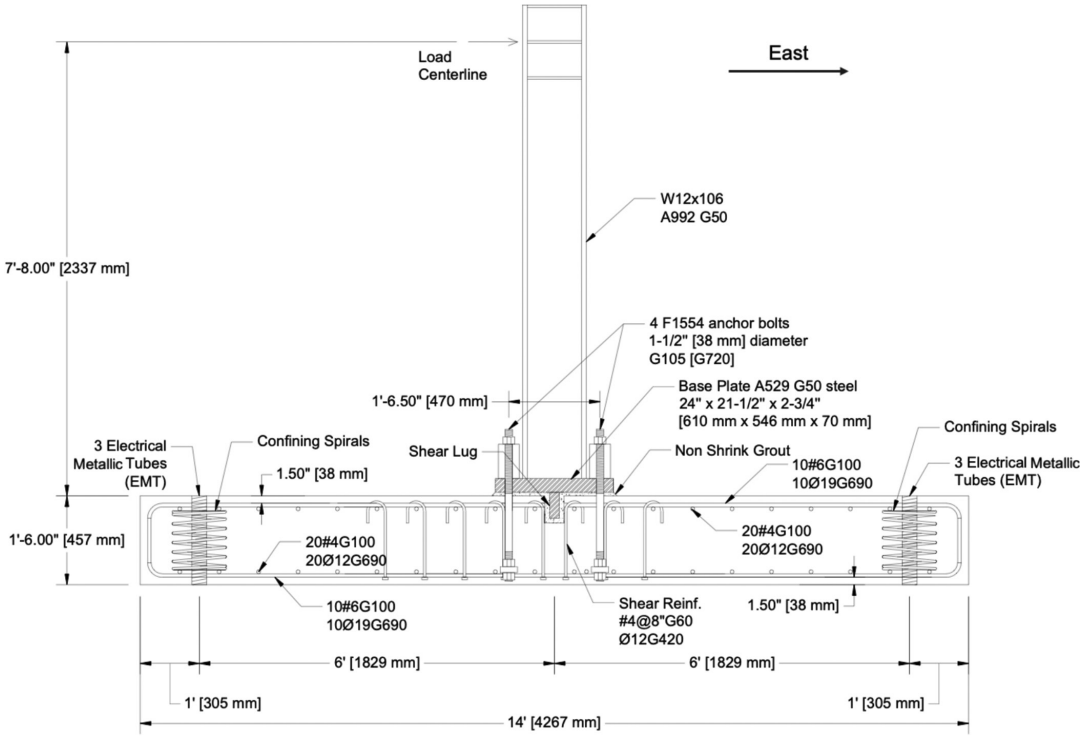

Fig. 6—Specimen M02 elevation view.

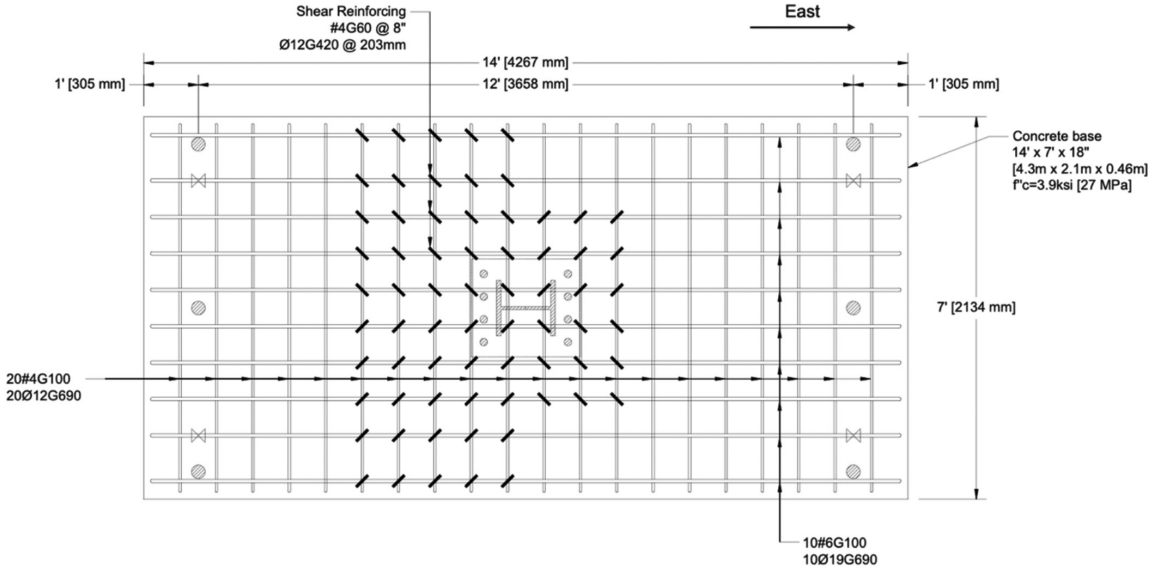

Fig. 7—Specimen M02 plan view.

Figure 9 summarizes the instrumentation for Specimen M01. A load cell was placed on each of the eight anchors. Thirty-three strain gauges were placed on the longitudinal reinforcement as shown. Two hoops were instrumented with a strain gauge at the midspan of each leg for a total of eight gauges. Two wire pots measured the column displacements at the elevation of the point of lateral force application in the north-south and east-west directions. Twenty-two vertical linear potentiometers measured the top surface displacement of the concrete slab and the base plate. Additional linear potentiometers monitored the sliding of the specimen and reaction blocks.

Test results—Specimen M01

Figure 10 shows the relationship between the column drift ratio and the force applied to the column free end. The drift ratio is defined as the displacement at the point of lateral force application divided by the height from the slab surface to the point of the force application. The initial relationship is nearly linear up to a lateral force approaching 50 kip (222 kN) in each loading direction, after which resistance increased only gradually with increasing displacement. The departure from nearly linear behavior was accompanied by flexural cracking in the slab and radial cracking along the top surface of the slab emanating from the anchor rods. The hysteresis loops show a pinching behavior.

Fig. 8—Test setup for both test specimens.

Figure 11 plots the relationship between the column drift ratio and the force in the anchor groups as measured by the load cells on each anchor. The east anchor group failed first during load step nine at a peak anchor group force of 249 kip (1070 kN) and a drift ratio of 1.5%. The west anchor group failed during the next load step (step 10) at a peak anchor group force of 266 kip (1080 kN) and a drift ratio of 2.1% (refer to Table 2). The anchor group failures were sudden and displaced a cone-shaped segment of concrete (refer to Fig. 12). After breakout failures, additional loadings show connection strength of approximately 50% of the peak strength in either direction (refer to Fig. 10). The first breakout failure did not seem to impact the strength of the second breakout failure as the peak forces in both directions were similar.

Figure 13 plots the column drift ratio against time and subdivides the drift ratio into contributions from the slab rotation, the relative base plate rotation, and the elastic column deflections due to moment and shear. The displacements due to the slab and the base-plate rotation are calculated based on displacements measured with the vertical linear potentiometers on the top surfaces. The column elastic deflection is calculated with elastic theory knowing the force applied to the column free end. Initially, most of the displacement is due to the elastic deformation of the column and the rotation of the base plate. Extension of the anchors is the major contributor to the base-plate rotation. As damage progresses in the concrete, the contribution of the slab rotation increases, while the contribution of the elastic column decreases. After the breakout failures, the displacement due to elastic column deflection decreases (due to the reduced force) and the slab rotation increases because the breakout cones displace like rigid objects.

Figure 14 plots the strains in each leg of a top and a bottom hoop against the column drift ratio (refer to the strain gauge and hoop location in Fig. 9). The strains in the bottom hoop did not exceed 50% of the yield strain. In the top hoop, only the legs that crossed the concrete cone failure planes show appreciable strain; that is, the legs in the east-west direction (H6 and H8). A "V" shape is observed as loading in both directions causes tensile strains in the hoops, which is expected.

Surface cracks indicated that the breakout cones were asymmetric with a steeper slope toward the interior of the joint (refer to Fig. 12). This cone geometry is attributed to the suppression of the unconstrained breakout surface because of flexural compression at the opposite side of the joint, as shown in Fig. 3. During the test, the longitudinal reinforcing bars and anchors remained in the elastic range. The bottom surface of the foundation slab showed minimal cracking. The anchors did not punch through the bottom of the slab. There was no evidence of joint crushing or joint dilation, as might be expected if there had been a beam-column joint failure.

Test specimen design—Specimen M02

Test Specimen M02 was designed so that strength would be limited by the failure of the concrete in the connection region. The steel column and base-plate fixture from the previous specimen were reused. Four 1-1/2 in. (38 mm) diameter anchor bolts (ASTM F1554 Grade 105) with 1.25 x 3.5 x 3.5 in. (32 x 89 x 89 mm) ASTM A36 steel plate washers were cast into the 18 in. (457 mm) thick foundation on each side of the column with an effective embedment depth from the top of the slab to the bearing surface of the plate washers equal to 14.3 in. (363 mm). The bearing plate was sized to keep the bearing stress below ACI 318-19 limits (Section 17.6.3.2.2). The bearing area of each plate was 9.8 in.^{2} (6350 mm^2).

The foundation slab was designed to resist the shear and moment resulting from developing the column moment yield strength. The same concrete mixture design was used as for the previous specimen. On test day, the measured compressive strength was 3930 psi (27.1 MPa). Other measured

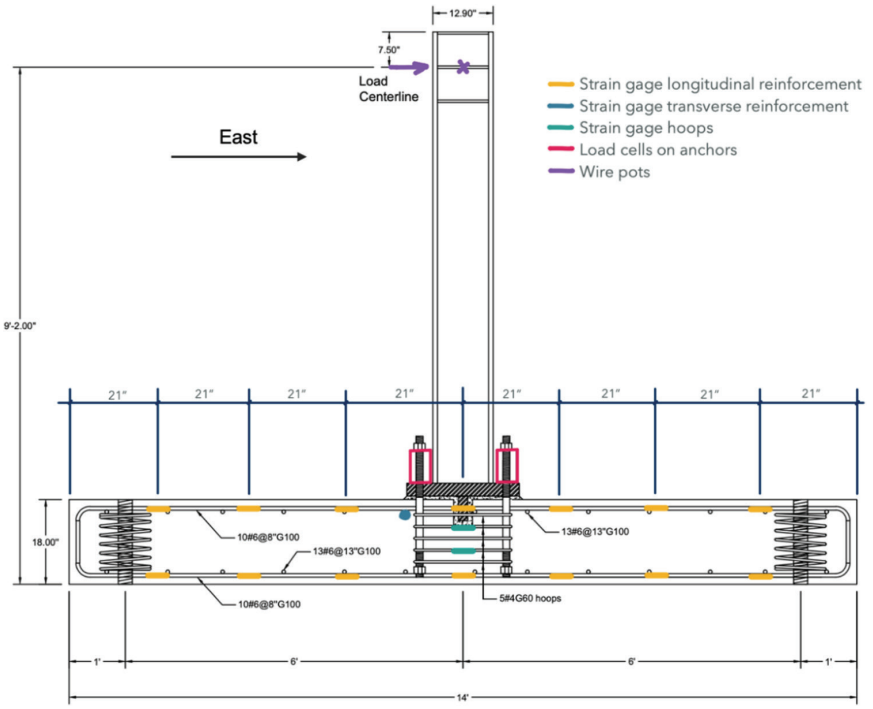

Fig. 9—Instrumentation as seen on east-west cut Specimen M01.

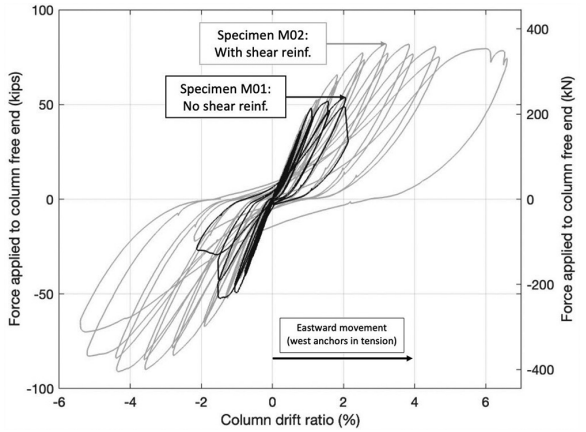

Fig. 10—Relationship between column drift ratio and force applied to column free end for both test specimens.

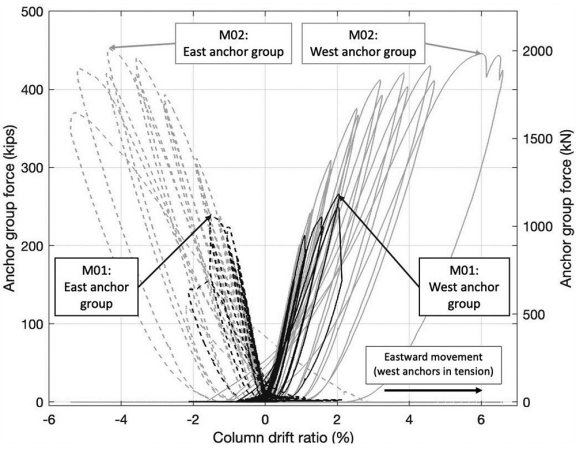

Fig. 11—Relationship between column drift ratio and force in anchor groups for both specimens.

material properties are shown in Table 1. The fracture energy (G_f) was measured with three-point bending tests following RILEM recommendations TC 50-FMC 1 (RILEM TC 50 1985). Refer to Worsfold and Moehle (2022) for further details on measured material properties, including stress-strain curves for concrete and reinforcing bars. Slab flexural reinforcement was sized assuming nominal yield strength f_y = 60,000 psi (420 MPa). However, Grade 100 (690 MPa) reinforcement was substituted to guard against yielding in case unexpected overloads or localized stress concentrations occurred. The shear reinforcement consisted of vertical No. 4 Grade 60 ASTM A706 bars (Ø13 mm Grade 420) in an 8 x 8 in. (203 x 203 mm) grid with 180-degree hooks on the top and heads on the bottom (refer to Fig. 6). The hook hung from the intersections of the longitudinal reinforcing mat and the head at the bottom was tied below the longitudinal steel. The shear reinforcement extended two rows farther on the west side than on the east side of the slab. No hoops were placed around the anchors.

The test setup for Specimen M02 was identical to Specimen M01 and was loaded in the same manner. The test was paused after each new displacement goal was reached to document cracking. Instrumentation similar to that of Specimen M01 was augmented by including strain gauges applied at the midheight of 34 of the shear reinforcing bars.

Test results—Specimen M02

Figure 10 shows the relationship between the column drift ratio and the force applied to the column free end. The initial relationship is nearly linear up to a lateral force approaching 50 kip (222 kN) in each loading direction, after which the force reached a plateau at approximately 80 kip (356 kN) in both directions. The departure from nearly linear behavior was accompanied by flexural cracking in the slab and radial

Table 2—Peak measured forces and drift ratios

Anchor group	Peak anchor group force, kip (kN)	Peak column lateral force, kip (kN)	Drift ratio at yield, DR_y, %	Drift ratio at max force, DR_{bo}, %
M01, east (failed first)	240 (1070)	52.3 (233)	1.1	1.5
M01, west (failed second)	266 (1180)	53.8 (239)	1.1	2.0
M02, east	452 (2010)	91.1 (405)	0.9	4.3
M02, west	446 (1980)	82.2 (366)	1.0	6.0

Note: For Specimen M02, yield drift ratio was taken as maximum drift ratio during load step seven. Drift ratio at failure was taken as drift ratio at maximum anchor force.

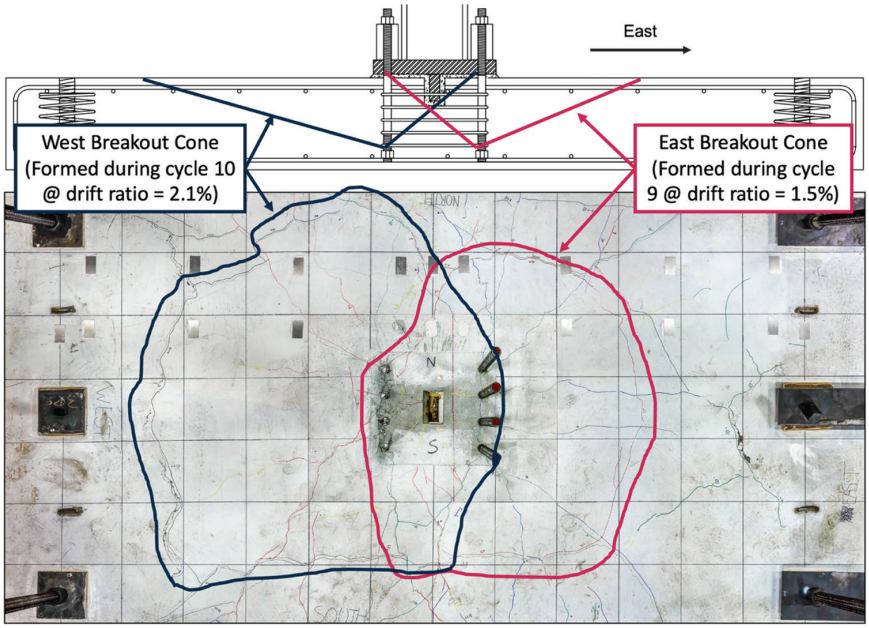

Fig. 12—Idealized cone geometry shown in elevation and observed cone geometry intersecting top surface in plan view, with 12 x 12 in. (305 x 305 mm) grid Specimen M01.

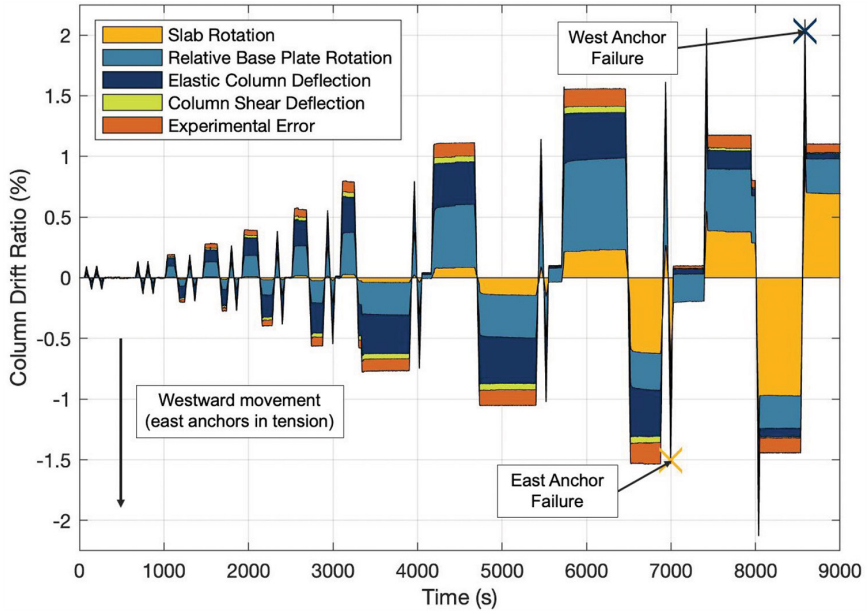

Fig. 13—Column drift ratio subdivided into contributions from slab rotation, relative base-plate rotation, elastic column deflection, column shear deflection, and experimental error versus time, Specimen M01.

cracking along the top surface of the slab emanating from the anchor rods. With a larger reinforced region, the west anchor group showed no drop in strength up to approximately a 6% drift ratio. In contrast, with a smaller reinforced region, the east anchor group began to lose strength after approximately a 4% drift ratio. The hysteresis loops show pinching.

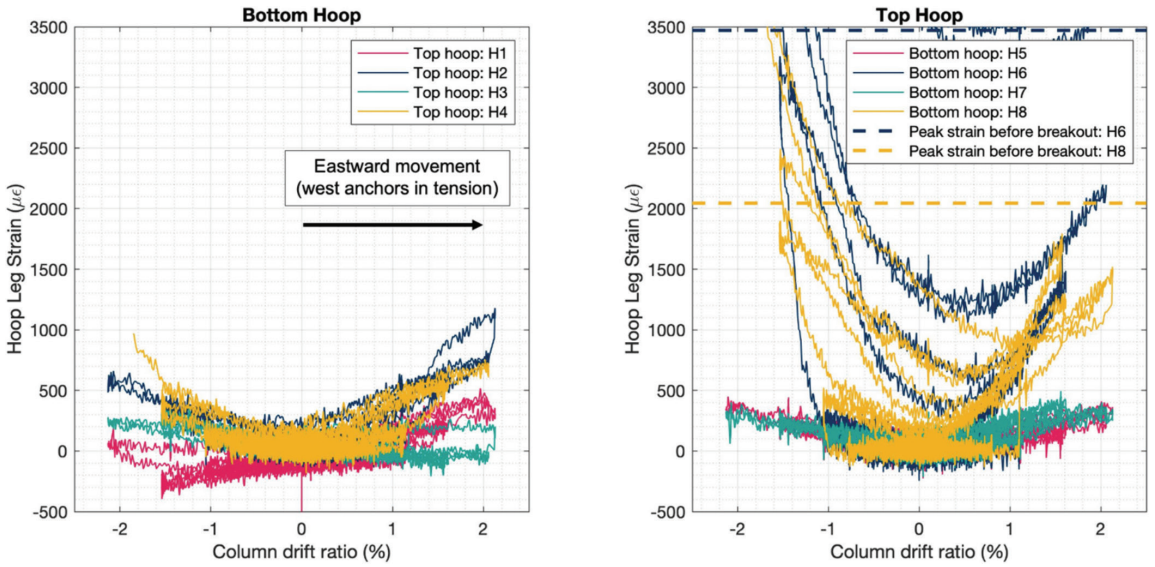

Fig. 14—Strains at midpoint of each leg of bottom and top hoops plotted against column drift ratio. Refer to strain gauge location in Fig. 9. Specimen M01.

Figure 11 plots the relationship between the column drift ratio and the force in the anchor groups as measured by the load cells on each anchor. Each anchor group failed by displacing a cone-shaped segment of concrete (refer to Fig. 15). The anchor group failure occurred more gradually than for Specimen M01. The peak force in the east group was 452 kip (2010 kN) and occurred at a drift ratio of 4.3%. The peak force in the west group was 446 kip (1980 kN) and occurred at a drift ratio of 6.0%.

Figure 16 plots the column drift ratio against time and subdivides the drift ratio into contributions from the slab rotation, the relative base-plate rotation, and the elastic column deflections due to moment and shear. The calculations were done in the same manner as for Specimen M01. Initially, most of the displacement is due to the elastic deformation of the column and the rotation of the base plate, which is due to elastic anchor extension. The contribution of the slab rotation increases as damage progresses in the concrete. Close to peak drift ratios, the slab rotation increases because the breakout cones have formed and move like rigid objects.

Figure 17 subdivides the shear reinforcing bars into rows based on the distance from the column center. Figure 17 also shows the final state of each bar, highlighting those that yielded. Most bars in rows 1 and 2 yielded and exceeded 3% strain (the maximum measurable strain of the strain gauge). The west side of the specimen had two additional rows of reinforcement (rows 4 and 5), which did not yield or show appreciable strains. Figure 18 plots the specimen force-drift ratio curve and highlights the point at which each shear reinforcing bar reached the nominal yield strain (0.002). The initiation of yielding of the shear reinforcement coincided with the departure from linear behavior of the specimen. Figure 19 plots the shear reinforcement strain versus column drift ratio and highlights the first yield of each bar. The "V" shape of the strain graphs indicates that the bars experienced tensile strains when the column was loaded in either direction.

Photographs of the specimen cross section (refer to Fig. 15) indicate that the breakout cones were asymmetric with a steeper slope toward the interior of the joint. This cone geometry is attributed to the suppression of the unconstrained breakout surface because of column flexural compression at the opposite side of the joint, as shown in Fig. 3. During the test, the longitudinal reinforcing bars and anchor rods remained in the elastic range. The bottom surface of the foundation slab showed minimal cracking. The anchors did not punch through the bottom of the slab.

DISCUSSION

Each specimen provided two data points corresponding to the failure of the east and west anchor groups. All four anchor groups failed in a concrete breakout mode. Other possible failure modes associated with slab flexure, one-way shear, or joint shear were not observed.

An analysis of the connection strength of test Specimen M01 was performed considering beam-column joint shear and anchoring-to-concrete provisions. The calculated strength using the strut-and-tie method is not presented because the bearing surfaces of the anchor bolts were not ideally positioned or sized for developing a proper strut-and-tie model.

The beam-column joint nominal shear strength was calculated with Eq. (1), assuming that the effective horizontal area of the joint was defined by lines located one nominal concrete cover dimension, or 1.5 in. (38 mm), outside the joint hoops of Specimen M01, resulting in

$$V_n = 15\sqrt{3700}\ (20.5\ \text{in.})(24\ \text{in.}) = 449\ \text{kip}\ (2000\ \text{kN}) \quad (9)$$

Assuming an internal moment arm in the foundation slab equal to $0.9d$ and ignoring self-weight, the corresponding horizontal column force can be calculated from equilibrium to be P = 86.4 kip (384 kN). Using AISC Design Guide 1 provisions (Fisher and Kloiber 2006), the internal moment

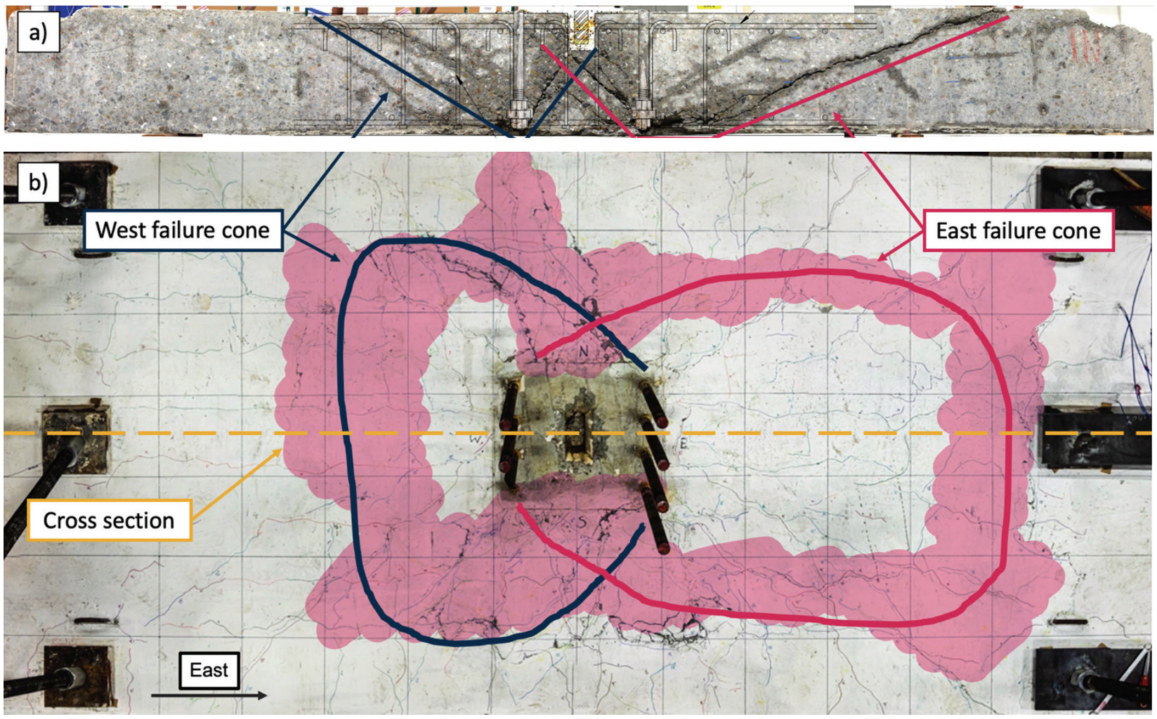

Fig. 15—(a) Specimen cross section; and (b) plan view highlighting crack patterns and breakout cone geometry, with 12 x 12 in. (305 x 305 mm) grid for Specimen M02. Shaded region produced hollow sound when knocked.

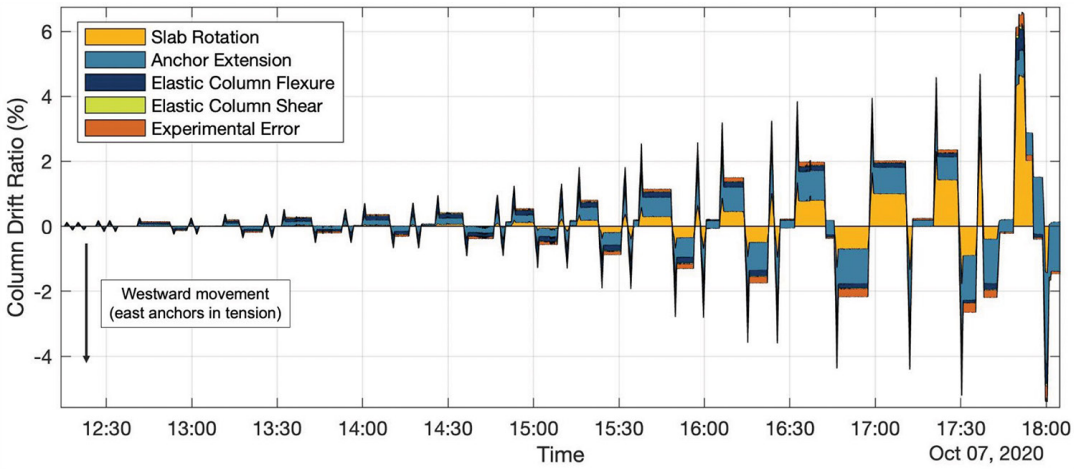

Fig. 16—Specimen M02 column drift ratio subdivided into contributions from slab rotation, relative base-plate rotation, elastic column deflection, column shear deflection, and experimental error versus time.

arm for the tension-compression couple of the base plate is z = 19.8 in. (502 mm). Thus, the force in the set of four anchor bolts in tension (T_n) corresponding to the nominal joint shear strength given by Eq. (9) is

$$T_n = PH/z = (86.4kN)(92 \text{ in.})/19.8 \text{ in.} = 402 \text{ kip } (1790 \text{ kN}) \quad (10)$$

where H is the vertical distance between the point of force application and the top surface of the slab.

The tensile capacity of the group of four anchor bolts was also calculated using the ACI 318-19 anchoring-to-concrete provisions. For this purpose, uncracked concrete is assumed as described previously. The additional factor Ψ_M from Eq. (7) is included to account for the proximity between the tensile and compressive forces (Fig. 3). The 1.33 factor is included to bring the 5% fractile anchor strength to the median value. The internal moment arm for the tension-compression couple of the base plate is calculated to be z = 20.5 in. (521 mm) using AISC Design Guide 1 procedures (Fisher and Kloiber 2006). Thus, using Eq. (4), the nominal median breakout capacity of the four anchor bolts in tension is

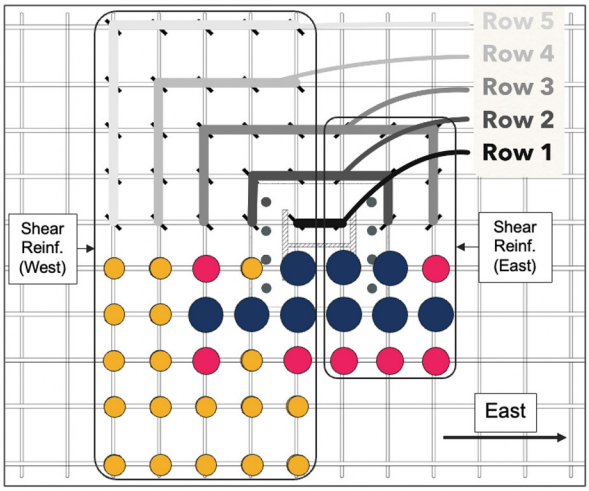

Marker	Bar State	Max Strain (μstrain)
	Elastic	0-2000
	Yielded	2000-31,000
	Damaged	>31,000

Notes:
- Shear reinforcing in rows 4 and 5 did not yield
- Strain gauges can measure up to about 3% strain

Fig. 17—Specimen M02 plan view showing final state of each instrumented bar and subdividing shear reinforcing into rows.

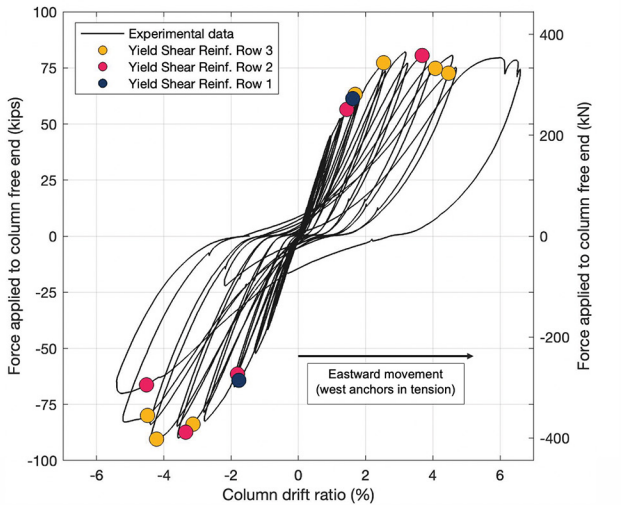

Fig. 18—Specimen M02 force versus drift ratio curve highlighting instances when shear reinforcing bars first reached nominal yield strain for Grade 60 (Grade 420) bars.

$$T_n = 1.33N_{cbg} = 1.33\frac{A_{Nc}}{A_{Nco}}\Psi_{ec,N}\Psi_{ed,N}\Psi_{c,N}\Psi_{cp,N}\Psi_M N_b$$

$$= 1.33\frac{2480\text{ in.}^2}{1840\text{ in.}^2}(1)(1)(1.25)(1)\left(2-\frac{20.5\text{ in.}}{1.5\cdot 14.3\text{ in.}}\right)$$

$$\left(16\sqrt{3700\text{ psi}}\right)(14.3\text{ in.})^{5/3} = 192\text{ kip (860 kN)} \quad (11)$$

Analogous calculations were performed for Specimen M02.

The calculated strengths and the measured values for Specimen M01 are summarized in Fig. 20. From the values given, it can be determined that the mean measured strength is approximately 1.3 times the strength calculated by the anchoring-to-concrete method, indicating that the mean breakout calculation is conservative for this case even with the inclusion of the Ψ_M adjustment. Comparison of the nominal breakout strength (5% fractile) without adjustment for the compression block (Ψ_M) yields a ratio of measured strength to calculated nominal strength of 1.8. Including the strength reduction factor $\phi = 0.70$, the ratio of measured to design strength becomes 2.6, and if the cracking factor $\Psi_{c,N}$ is taken equal to 1.0, as may be inferred from the language in ACI 318-19, then the ratio of measured peak strength to design strength rises to 3.3. On the other hand, the beam-column joint shear calculation yields a ratio of mean measured strength to nominal strength based on the beam-column joint nominal shear strength of 0.62, indicating that failure occurred well before the nominal joint shear strength was reached.

This example demonstrates the conservatism of the anchoring-to-concrete provisions for large-scale column-foundation connections as specified in ACI 318-19. The use of a 5% fractile value for the design of concrete anchors is rooted in concerns about risk and failure consequences associated with attachments anchored by one or a small number of anchors where force redistribution is unlikely, and failure is sudden. When used to design large structural elements anchored by multiple anchor groups, the provisions result in a higher degree of conservatism than is commonly provided for similar connections with hooked or headed reinforcing bars. The use of a median strength value, rather than a 5% fractile, should be considered along with an appropriate strength reduction factor for anchors used in structural applications.

Strain gauge data from Specimen M01 indicate that the joint hoops were not effective in confining the joint or increasing the breakout strength. For the bottom hoop, Fig. 14 shows low strains in all legs. For the top hoop, only the two legs that crossed the cone failure plane yielded.

Specimen M02 incorporated an 8 x 8 in. (203 x 203 mm) shear reinforcing grid of No. 4 Grade 60 (Ø13 mm Grade 420) bars with a 180-degree hook on one side and a head on the other. Both ends engaged longitudinal reinforcement. After controlling for concrete strength, the addition of shear reinforcement in Specimen M02 increased the breakout force by 72% and the displacement capacity by a factor of 3 on average compared to Specimen M01 (refer to Table 2). The increased peak force is comparable to the calculated beam-column joint strength (refer to Fig. 20). The strength increase is consistent with the strut-and-tie model developed by Kupfer et al. (2003) for column-foundation connections, which suggests tension ties outside the joint are required for

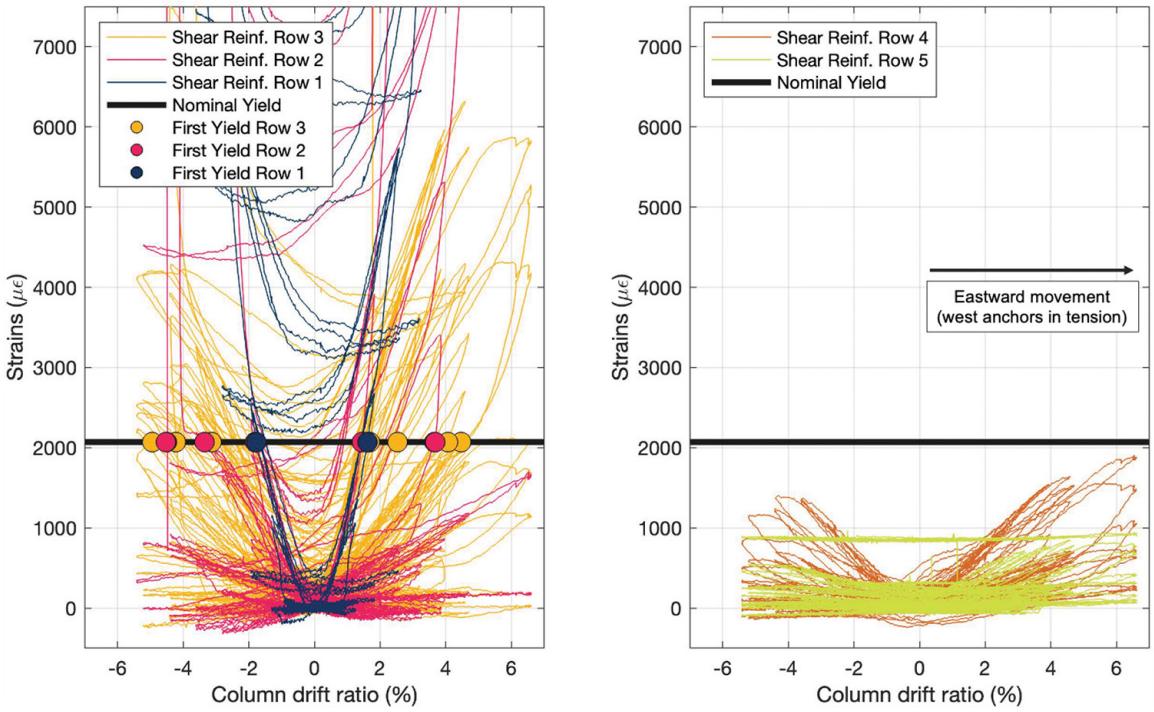

Fig. 19—Specimen M02 strain in shear reinforcing bars versus column drift ratio subdivided into rows. First yield of each bar is highlighted.

equilibrium. Contrary to the current assumptions in the ACI 318-19 and EN 1992-4:2018 design equations, relatively small amounts of shear reinforcement can improve the connection behavior. Most shear bars near the anchors developed strains well beyond the nominal yield strain (>3%) even though they were not fully developed on both sides of the potential breakout cone as would be required for ACI 318-19 anchor reinforcement. This observation suggests that anchoring shear reinforcing bars following the requirements for transverse reinforcement (ACI 318-19, Section 25.7.1.3) may be sufficient to develop the nominal yield stress.

Both specimens exhibited pinched hysteresis loops (refer to Fig. 10), indicating a non-ductile concrete breakout failure mode similar to those observed by Tanaka and Oba (2001). Increasing the breakout failure strength may allow the designer to provide an alternate, more ductile failure mode (for example, anchor or column yielding).

For the east anchor group of Specimen M02, the east face of the failure cone is located beyond the outer perimeter of the shear reinforcing bars (refer to Fig. 15). If one assumes the shear reinforcing bars form part of the anchor group, the calculated strength of this larger secondary breakout cone increases by a factor of 1.71 due to the increased group factor. This strength increase is almost exactly that observed between Specimens M01 and M02 (72%). The calculated increase in strength for a breakout cone beyond the shear reinforcement on the west side is approximately 3.14 due to the larger reinforced area. This potential breakout cone was not observed.

The additional rows of shear reinforcement on the west side of test Specimen M02 did not increase the load capacity but did increase the displacement capacity from a drift ratio of approximately 4% to approximately 6% and prevented the formation of a secondary breakout cone initiating where the shear reinforcement ended. The observation that stirrups beyond $0.75h_{ef}$ from the anchor centerline did not increase the anchor force is consistent with Eurocode provisions for effective supplementary reinforcement (EN 1992-4:2018 Section 7.2.1.2 (2) c)).

Neither specimen showed substantial cracking along the bottom surface. This suggests that the absence of continuous soil pressure under the test specimens did not have a substantial effect on the observed concrete breakout failure mode which governed the strength. The influence of soil support on other failure mechanisms should be investigated further.

For both specimens, the failure cones were asymmetric with a steeper slope toward the interior of the joint (refer to Fig. 12 and 15). This cone geometry is attributed to the suppression of the unconstrained breakout surface because of flexural compression at the opposite side of the joint, as shown in Fig. 3. The Ψ_M factor from Eq. (7) seems appropriate to account for the breakout strength increase associated with the flexural compression force. This factor requires the calculation of the internal lever arm (z). This value can be approximated by either: a) assuming the compression resultant is located below the column flange (z = 15.2 in. [386 mm] and Ψ_M = 1.29); b) assuming the compression resultant is located at the opposite edge of the base plate (z = 21.25 in. [540 mm] and Ψ_M = 1.01); or c) assuming uniform bearing pressure below the base plate and calculating z from the forces applied to the column following AISC Design Guide 1 recommendations (Fisher and Kloiber 2006) (z = 20.5 in. [521 mm] and Ψ_M = 1.04)(1.4 for both specimens). Figure 21 plots the measured anchor group forces versus those calculated following AISC recommendations. During early load cycles, the measured and theoretical values are similar, but

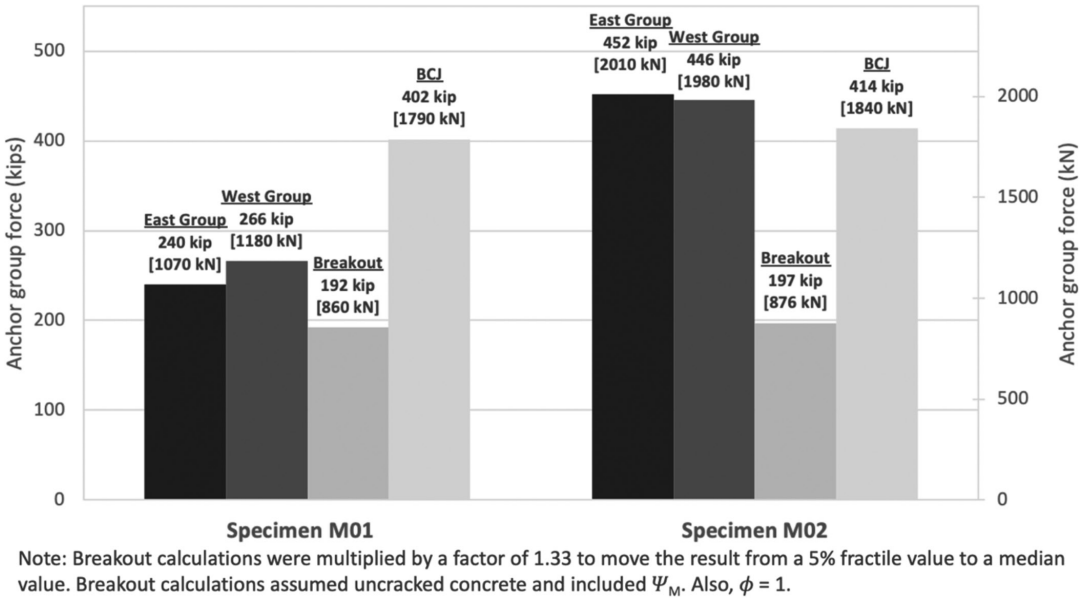

Fig. 20—Experimental peak anchor forces and nominal median values according to breakout equations and beam-column joint (BCJ) shear equations.

as the test progresses, the measured values become larger. At failure, the measured forces are approximately 15 to 20% higher than those calculated assuming a uniform bearing pressure, suggesting this method may overestimate z and result in a conservative value of Ψ_M. Measuring z from the centroid of the tensile anchors to the far edge of the base plate may be assumed as a conservative and straightforward approximation unless a more detailed calculation is performed. The stiffer the base plate, the more accurate this assumption will be.

ACI 318-19 Commentary Section R25.4.4.2c suggests that breakout failure in a beam-column joint can be precluded by keeping anchorage length greater than or equal to 1/1.5 times the effective depth of the member introducing the anchor force into the joint, presumably due to the restraining influence of the compression field. However, for both test specimens, breakout failure occurred even though this recommendation was satisfied.

Designing Specimen M01 considering only the beam-column joint strength and ignoring breakout strength would have been unconservative (refer to Fig. 20). The ratio of nominal breakout strength to nominal joint shear failure was on the order of 2.1. This observation suggests that both failure modes, breakout and joint shear, should be checked to produce safe designs.

With additional shear reinforcement, the breakout failure force of Specimen M02 became comparable to the beam-column joint strength. The experiments did not test whether further additions of shear reinforcement would result in further increases in strength or whether strength would be limited by beam-column joint shear strength. The formation of a secondary failure cone beyond the outer perimeter of the shear reinforcement, analogous to the requirement for two-way slabs with shear reinforcement, should also be considered.

SUMMARY AND CONCLUSIONS

Two full-scale test specimens of interior steel-column-to-concrete-foundation connections with cast-in-place anchor bolts were constructed and tested. Each test specimen provided two data points corresponding to the peak forces of each anchor group. The columns were tested under incrementally increasing cyclic lateral loading, resulting in moment transfer from the column to the foundation element. All four tested anchor groups failed in a brittle concrete breakout mechanism due to tensile force transfer from the anchor bolts to the foundation. This observation challenges the assumption that breakout failures will not govern the behavior of large-scale connections, provided they have adequate joint shear capacity. The pinched hysteresis loops are indicative of concrete failure. There was no evidence of failure or distress associated with other force-limiting mechanisms.

For Specimen M01 without shear reinforcement, the nominal breakout strength of the tension anchor bolt group was calculated using the anchoring-to-concrete provisions of ACI 318-19. The measured breakout strength was 1.8 times the Code-based nominal strength, indicating the conservatism of the ACI 318-19 provisions for this case. Part of the conservatism is because the ACI 318-19 provisions for anchoring to concrete take the 5% fractile of resistance for design rather than the median value, as is more common for other nominal strengths. ACI 318-19 also currently neglects the positive influence of the flexural compression field developed under the base plate, which can act to retard the formation of the concrete breakout surface. Finally, the ACI 318-19 provisions are written to suggest that strength should be calculated considering cracked concrete ($\Psi_{c,N}$ equal to 1.0), even though an assumption of uncracked concrete ($\Psi_{c,N}$ equal to 1.25) may be justified for headed anchors if the bearing surface of the anchor bolt is within the flexural

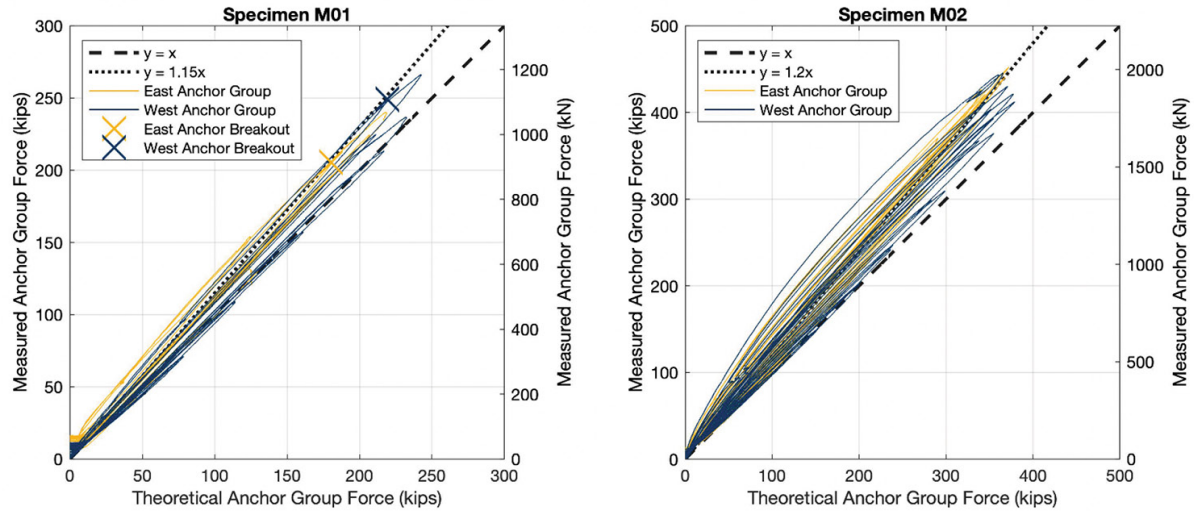

Fig. 21—Comparison between measured and theoretical and anchor group forces. Measured forces were obtained from load cells on anchors. Theoretical forces were calculated using AISC Design Guide 1 uniform bearing pressure model.

compression region of the foundation. These three effects should be considered in future revisions to ACI 318.

Calculations for test Specimen M01 also demonstrated that the beam-column joint shear strength was never realized because it was preempted by tension breakout failure. For Specimens M01 and M02, the breakout failure governed even though the anchorage length was greater than 1/1.5 times the effective depth of the member introducing the anchor force into the joint. This observation runs contrary to ACI 318-19 Commentary Section R25.4.4.2. ACI 318 should consider revised guidance or new Code requirements emphasizing the importance of checking breakout failures in addition to checking joint shear strength. A good practice would be to check both breakout strength and beam-column joint shear strength and use the lower value as the limit for design. This observation may also be relevant for beam-column joint design.

The addition of a distributed grid of shear reinforcement in the breakout cone region can increase the breakout strength and displacement capacity. Increasing the breakout strength may allow the designer to provide a more desirable ductile failure mode like anchor yielding. Even though only the shear reinforcement within $0.75h_{ef}$ of the anchors seems capable of increasing the breakout strength, additional rows can increase the displacement capacity and prevent secondary breakout failure cones beyond the outermost row of shear reinforcement. ACI 318 and the Eurocodes should consider including provisions that combine the strength of concrete and shear reinforcement for the concrete breakout failure mode.

AUTHOR BIOS

ACI member **Benjamin L. Worsfold** *is a T. Y. Lin Fellow and PhD Candidate in the Structural Engineering, Mechanics and Materials program at the University of California, Berkeley (UC Berkeley), Berkeley, CA. He received his BS in civil engineering from the University of Costa Rica, San Pedro de Montes de Oca, SJ, Costa Rica, in 2015, and his MS from UC Berkeley in 2017. He is a member of ACI Subcommittee 318-1R, Resolution of Anchorage and Development Provisions. His research interests include anchoring to concrete, laboratory testing, and finite element analysis of reinforced concrete.*

Jack P. Moehle, *FACI, is a Professor in the Graduate School at UC Berkeley. He is past Chair of ACI Committee 318, Structural Concrete Building Code, and a past member of the ACI Board of Direction and Technical Activities Committee.*

John F. Silva, *FACI, is a Licensed Structural Engineer in California and Senior Director of Codes and Standards for Hilti North America.*

ACKNOWLEDGMENTS

The authors express their gratitude to the ACI Foundation Concrete Research Council, AISC, and Hilti Corporation for financing this and other ongoing research projects at UC Berkeley relating to concrete anchorage. Special thanks to R. Klemencic, Chairman and CEO of Magnusson Klemencic Associates; Level 10 Construction; Cascade Steel; and PJ's Rebar, Inc., for donations of materials and manual labor. This study was greatly improved through discussions with the following individuals: R. Sabelli (Director of Seismic Design at Walter P Moore), J. Malley (Senior Principal of Degenkolb Engineers), and Dr. R. Piccinin (Vice President for Code Development and Research at Hilti Corporation).

NOTATION

A_{cs}	=	cross-sectional area at end of strut under consideration
A_j	=	cross-sectional area of horizontal plane through joint, in.^{2}
A_{Nc}	=	projected failure area of single anchor or anchor group in question
A_{Nco}	=	projected concrete failure area of single anchor if not affected by edges ($9h_{ef}^2$)
A_{nz}	=	area of each face of nodal zone
DR_{bo}	=	drift ratio at breakout failure
DR_y	=	drift ratio when leaving elastic range
d	=	distance between extreme compression fiber to centroid of longitudinal tension reinforcement
E	=	concrete modulus of elasticity
F_{nn}	=	nominal compressive strength of nodal zone
F_{ns}	=	nominal axial compressive strength of strut
f_c'	=	concrete compressive strength
f_{mean}	=	conversion factor from 5% fractile to median value
f_t	=	concrete tensile strength
f_y	=	nominal yield stress of steel
G_f	=	concrete fracture energy
H	=	vertical distance between top surface of slab and point force is applied
h_{ef}	=	anchor effective embedment depth
N_b	=	basic concrete breakout strength of single anchor in tension in cracked concrete
N_{cbg}	=	nominal concrete breakout strength in tension of group of anchors
P	=	horizontal force applied to column free end
T_n	=	tensile force in anchor group
V_n	=	nominal horizontal joint shear strength
z	=	lever arm between tensile and compressive force resultants

β_c = strut and node confinement modification factor for strut-and-tie method
β_n = nodal zone coefficient for strut-and-tie method
β_s = strut coefficient for strut-and-tie method
ϕ = strength reduction factor
γ = joint shear strength coefficient that depends on joint geometry and loading
$\Psi_{c,N}$ = modification factor for anchors in uncracked concrete under service loads
$\Psi_{cp,N}$ = modification factor for concrete splitting with post-installed anchors
$\Psi_{ec,N}$ = modification factor for anchor groups loaded eccentrically in tension
$\Psi_{ed,N}$ = modification factor for edge effects of anchors in tension
Ψ_M = modification factor for bearing pressure of base plate by Herzog (2015)

REFERENCES

ACI Committee 318, 2019, "Building Code Requirements for Structural Concrete (ACI 318-19) and Commentary (ACI 318R-19)," American Concrete Institute, Farmington Hills, MI, 624 pp.

Bažant, Z. P., 2000, "Size Effect," *International Journal of Solids and Structures*, V. 37, No. 1-2, Jan., pp. 69-80. doi: Elsevier Science Ltd.10.1016/S0020-7683(99)00077-3

Caltrans, 2016, "Memo to Designers (MTD) 20-7: Seismic Design of Slab Bridges," California Department of Transportation, Sacramento, CA, Apr., 12 pp.

Eligehausen, R., and Balogh, T., 1995, "Behavior of Fasteners Loaded in Tension in Cracked Reinforced Concrete," *ACI Structural Journal*, V. 92, No. 3, May-June, pp. 365-379.

Eligehausen, R.; Bouška, P.; Červenka, V.; and Pukl, R., 1992, "Size Effect of the Concrete Cone Failure Load of Anchor Bolts," *Fracture Mechanics of Concrete Structures*, Z. P. Bažant, ed., Taylor & Francis Group, London, UK, pp. 517-525.

Eligehausen, R.; Mallée, R.; and Silva, J. F., 2006, *Anchorage in Concrete Construction*, Ernst & Sohn, Berlin, Germany, 391 pp.

EN 1992-4:2018, 2018, "Eurocode 2 – Design of Concrete Structures – Part 4: Design of Fastenings for Use in Concrete," European Committee for Standardization, Brussels, Belgium, 129 pp.

Fisher, J. M., and Kloiber, L. A., 2006, "Steel Design Guide 1: Base Plate and Anchor Rod Design," second edition, American Institute of Steel Construction (AISC), 63 pp.

Fuchs, W.; Eligehausen, R.; and Breen, J. E., 1995, "Concrete Capacity Design (CCD) Approach for Fastening to Concrete," *ACI Structural Journal*, V. 92, No. 1, Jan.-Feb., pp. 73-94.

Herzog, M., 2015, "Beitrag zur Vereinheitlichung der Bemessung im Stahlbetonbau und in der Befestigungstechnik (Contribution to the Standardization of Design in Reinforced Concrete Construction and Fastening Technology)," PhD dissertation, University of Stuttgart, Stuttgart, BW, Germany, 457 pp. (in German)

Joint ACI-ASCE Committee 352, 2002, "Recommendations for Design of Beam-Column Connections in Monolithic Reinforced Concrete Structures (ACI 352R-02) (Reapproved 2010)," American Concrete Institute, Farmington Hills, MI, 38 pp.

Kupfer, H.; Münger, F.; Kunz, J.; and Jähring, A., 2003, "Hauptaufsätze – Nachträglich verankerte gerade Bewehrungsstäbe bei Rahmenknoten (Anchorage of Post Installed Straight Bars for Frame Node Connections)," *Bauingenieur*, V. 78, No. 1, pp. 24-37. (in German)

Mahrenholtz, C.; Akguzel, U.; Eligehausen, R.; and Pampanin, S., 2014, "New Design Methodology for Seismic Column-to-Foundation Anchorage Connections," *ACI Structural Journal*, V. 111, No. 5, Sept.-Oct., pp. 1179-1189.

Nilforoush, R.; Nilsson, M.; and Elfgren, L., 2018, "Experimental Evaluation of Influence of Member Thickness, Anchor-Head Size, and Orthogonal Surface Reinforcement on the Tensile Capacity of Headed Anchors in Uncracked Concrete," *Journal of Structural Engineering*, ASCE, V. 144, No. 4, Apr., p. 04018012. doi: 10.1061/(ASCE)ST.1943-541X.0001976

Nilforoush, R.; Nilsson, M.; Elfgren, L.; Ožbolt, J.; Hofmann, J.; and Eligehausen, R., 2017, "Influence of Surface Reinforcement, Member Thickness, and Cracked Concrete on Tensile Capacity of Anchor Bolts," *ACI Structural Journal*, V. 114, No. 6, Nov.-Dec., pp. 1543-1556. doi: 10.14359/51689505

Ožbolt, J.; Elighausen, R.; and Reinhardt, H. W., 1999, "Size Effect on the Concrete Cone Pull-Out Load," *International Journal of Fracture*, V. 95, No. 1-4, Jan., Article No. 391. doi: 10.1023/A:1018685225459

Papadopoulos, V.; Murcia-Delso, J.; and Shing, P. B., 2018, "Development of Headed Bars in Slab-Column Joints of Reinforced Concrete Slab Bridges," *ACI Structural Journal*, V. 115, No. 5, Sept., pp. 1393-1406. doi: 10.14359/51702247

RILEM TC 50, 1985, "FMC 1: Determination of the Fracture Energy of Mortar and Concrete by Means of Three-Point Bend Tests on Notched Beams," *Materials and Structures*, V. 18, No. 4, July, pp. 287-290.

RILEM TC 89, 1994, "FMC 2: Size-Effect Method for Determining Fracture Energy and Process Zone Size of Concrete," *RILEM Technical Recommendations for the Testing and Use of Construction Materials*, E & FN Spon, London, UK, pp. 102-106.

Sharma, A.; Eligehausen, R.; and Asmus, J., 2017a, "Comprehensive Analytical Model for Anchorages with Supplementary Reinforcement," Proceedings, 3rd International Symposium on Connections between Steel and Concrete (ConSC 2017), Sept. 27-29, Stuttgart, Germany, pp. 253-265

Sharma, A.; Eligehausen, R.; and Asmus, J., 2017b, "Comprehensive Experimental Investigations on Anchorages with Supplementary Reinforcement," Proceedings, 3rd International Symposium on Connections between Steel and Concrete (ConSC 2017), Sept. 27-29, Stuttgart, Germany, pp. 242-252

Tanaka, R., and Oba, K., 2001, "Experimental Study on Seismic Performance of Beam Members Connected with Post-Installed Anchors," *International Symposium on Connections between Steel and Concrete*, R. Eligehausen, ed., Stuttgart, Germany, RILEM Publications SARL, pp. 576-585.

Worsfold, B., and Moehle, J., 2019, "Laboratory Tests of Column-Foundation Moment Transfer Connections with Headed Anchors," UCB/SEMM-2019/01, Structural Engineering, Mechanics and Materials (SEMM) Report, University of California, Berkeley, Berkeley, CA, 171 pp.

Worsfold, B., and Moehle, J., 2022, "Laboratory Tests of Column-Foundation Moment Transfer Connections with Shear Reinforcement," UCB/SEMM-2022/01, Structural Engineering, Mechanics and Materials (SEMM) Report, University of California, Berkeley, Berkeley, CA, 243 pp.